Australian Meteorological and Oceanographic Journal 63 (2013) 325–338

Rainfall distribution of five landfalling tropical cyclones in the northwestern Australian region

Yubin Li[1], Kevin K.W. Cheung[1], Johnny C.L. Chan[2], and Masami Tokuno[3]
[1]Department of Environment and Geography, Macquarie University, Sydney, Australia
[2]Guy Carpenter Asia-Pacific Climate Impact Centre, School of Energy and Environment, City University of Hong Kong, Hong Kong
[3]Meteorological Research Institute/Japan Meteorological Agency, Tsukuba, Ibaraki, Japan

(Manuscript received July 2012; revised December 2012)

Rain gauge data, satellite IR brightness temperature and radar-estimated rain rate for five tropical cyclones from the 2005–06 to 2009–10 seasons that made landfall along the northwestern coast of Australia are analysed. It is the first time that the spatial rainfall distribution of landfalling tropical cyclones in the southern hemisphere has been systematically investigated. It is found that the distributions of rainfall are more concentrated in the right side of the track of the landfall tropical cyclones, which is the offshore flow position. Potential mechanisms responsible for this observed asymmetry in rainfall distribution are discussed. These include the tropical cyclone motion direction, deep-tropospheric vertical wind shear and land-sea contrast in surface properties. Topography is considered to have less effect since Western Australia is relatively flat. The rainfall maxima are found in the front and downshear quadrants for these tropical cyclones, which is consistent with previous studies. The changes in vertical wind shear when these tropical cyclones moved to the south are largely attributed to the prevailing environmental flow. Three numerical simulations are performed; one with a realistic land surface, one with all topography removed and one with all land removed. These simulations show that the land surface effects play an important role in determining the asymmetry in rainfall distribution, which explains why in some cases the observed maximum rainfall does not follow closely the vertical wind shear direction when making landfall.

Introduction

Torrential rainfall brought by landfalling tropical cyclones often causes huge losses to human life and property. It was reported that freshwater floods have caused more than one-half of the 600 casualties in the United States directly associated with tropical cyclones or their remnants during 1970–1999 (Rappaport 2000). Australian examples include the hazardous impacts from tropical cyclone *Larry* (2006) and tropical cyclone *Yasi* (2011) to the State of Queensland, and tropical cyclone landfalls were responsible for an average of four casualties per year during the 1960–1989 period (Ryan 1993). Knowledge of the region along the coast where the heaviest precipitation will be experienced is therefore crucial to reduce the losses (Chan et al. 2004). However, the rainfall patterns in tropical cyclones are complex and vary from case to case (Lonfat et al. 2007). Rainfall forecasts of landfalling tropical cyclones are further complicated by the coastal and inland topography as well as by the land surface and boundary layer conditions, which often lead to distinct rainfall asymmetries (May et al. 2008, Gao et al. 2009).

Early studies based on rain gauge data found that coastal rainfall associated with tropical cyclones is generally more intense to the right side of the tracks of northern hemisphere tropical cyclones (Koteswaram and Gaspar 1956, Miller 1958). Recent numerical studies (e.g. Chen and Yau 2003) and observational studies (e.g. Yuan et al. 2009 using radar data) of northern hemisphere tropical cyclones at landfall also indicated that the convection was concentrated in the

Corresponding author address: Kevin Cheung, Department of Environment and Geography, Macquarie University, Sydney, NSW, 2109, Australia. Email: Kevin.Cheung@mq.edu.au

front-right quadrant with respect to motion vector. Dunn and Miller (1960) suggested that low-level convergence to the right of a northern hemisphere tropical cyclone track is more likely to be enhanced by the increased surface friction during landfall, and hence more rainfall. This idea was supported by observations (Powell 1982, 1987) as well as numerical simulations (Tuleya and Kurihara 1978, Jones 1987). However, the rainfall maxima appeared to the left side of the northern hemisphere tropical cyclone tracks in some other cases. For example, the radar-derived total rainfall maximum was found to the left of hurricane *Frederic's* (1979) track (Parrish et al. 1982). The same characteristic was found in the landfall of hurricane *Danny* (1997; Blackwell 2000). An f-plane simulation study of northern hemisphere tropical cyclone landfall by Chan and Liang (2003) also identified maximum rainfall in the front and left quadrants prior to landfall. However, if land surface moisture flux is cut off and surface roughness is increased, the maximum rainfall shifts toward the front and right quadrants.

Not much research has been conducted on landfalling tropical cyclones in the southern hemisphere. For the northwest Australian region (0°–35°S, 105°–135°E), the annual mean tropical cyclone occurrence is 5.6 (standard deviation of 2.3; Goebbert and Leslie 2010). The mean number of tropical cyclone landfalls in the same region is 1.5 (out of 4.9 for all Australian coastlines; Dare and Davidson 2004). Dare and Davidson (2004) also showed that while most sections of the northern half of the Australian coastline have been subjected to tropical cyclones making landfall, there are more landfalls in the northwestern region associated with tropical cyclones having attained category 3 to 5 intensity in their lifetimes. One recent numerical study of tropical cyclone *Larry* (2006) that made landfall on the northeastern coast of Australia showed that the rainfall to the right side was heavier than to the left side of the tropical cyclone track during landfall (Ramsay and Leslie 2008). However, with topography removed the opposite result occurred.

It is widely accepted that increased surface friction due to tropical cyclone transition will lead to front-right (front-left) maximum convergence for northern hemisphere (southern hemisphere) tropical cyclones (Shapiro 1983, Kepert 2001, Kepert and Wang 2001). However, since rainfall asymmetries are affected by multiple factors including but not limited to tropical cyclone motion, topography, surface roughness and heat fluxes, vertical wind shear (VWS) and environmental flow, the rainfall distribution can be highly variable among different tropical cyclones. By using satellite, radar and global reanalysis data, this study identifies the rainfall asymmetries of five southern hemisphere tropical cyclones that made landfall along the northwestern coast of Australia, and the possible mechanisms for the characteristics of the rainfall distribution are discussed. In order to verify the land-sea contrast effect, numerical simulations for tropical cyclone *Glenda* (2006) are conducted. The data used in this paper and the model configuration are described in 'Data and model configuration', while the general description of the evolution and tracks of the tropical cyclones are in 'General description of tropical cyclones'. 'Asymmetries in convection and rainfall distributions' presents the analysis of the rainfall asymmetries during landfall. The final section discusses possible mechanisms with supports from the simulation results to explain the asymmetric rainfall distributions, followed by a summary and concluding remarks.

Data and model configuration

The best track data of the tropical cyclones is from the Australian Bureau of Meteorology (http://www.bom.gov.au/cyclone/history/index.shtml). Other observational data include the Australian Water Availability Project (AWAP) gridded daily rainfall from the Bureau (http://www.bom.gov.au/jsp/awap/rain/). The AWAP gridded daily rainfall is gauge observation-based and interpolated to 0.05° latitude/longitude girds. Radar-estimated rain rate is from the northwestern area radar stations of the Australian Weather Watch Radar Network. The radar stations involved are located at Wyndham, Broome, Port Hedland, Dampier, Learmonth and Carnarvon (see locations in Fig. 1). These radars have a typical range of 256 km, and the maximum range is 512 km. The radar data are expressed in polar coordinates with 1° resolution in azimuthal angle and 2 km resolution in range. Temporal resolution of the radar data is 10 min. Radar-estimated rain rate is categorised into 16 levels from level 0 indicating a rain rate under 2 mm h^{-1} to level 15 indicating a rain rate over 360 mm h^{-1}. For locations that have rain rate estimated by more than one radar station at the same time, the radar data that indicate the strongest rain rate are used.

Fig. 1. Observed six-hourly positions of tropical cyclones *Glenda* (2006), *George* (2007), *Nicholas* (2008), *Billy* (2009) and *Laurence* (2010) during the periods indicated in the legends. The black dots indicate the locations of the radars, and dashed circles indicate a distance of 256 km from each radar station.

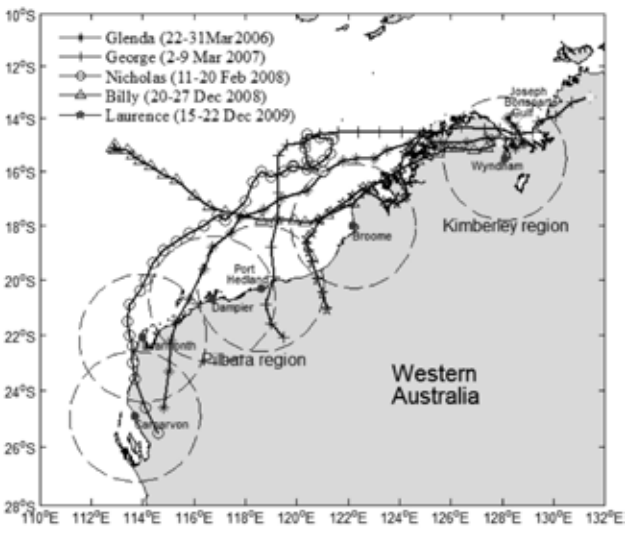

The infrared (IR) brightness temperatures (TB) from the Multifunctional Transport Satellite (MTSAT) are used to monitor the development of deep convection. The MTSAT images have temporal resolution of one hour and horizontal resolution of 0.05° latitude/longitude. In particular, the areas with TBs less than –75 °C are identified as deep convection (Lee et al. 2008).

For synoptic analysis and calculating VWS, the wind components from the Climate Forecast System Reanalysis (CFSR) of the National Centers for Environmental Prediction (NCEP) are applied. The CFSR has a spatial resolution of 0.5° latitude/longitude, and temporal resolution of six hours.

Version 3.3 of the Weather Research and Forecasting (WRF) model developed by the US National Center for Atmospheric Research is used to simulate the tropical cyclones. The simulations are performed on two-way interactive grids with the nested domain moving along with the vortex centre. The two domains (indicated in Fig. 10) have horizontal resolutions of 9 km and 3 km, respectively. There are 35 vertical half-sigma levels with model top at 50 hPa. The initial (including the tropical cyclone vortex without additional bogus) and lateral boundary conditions are obtained from the NCEP Final Analysis (FNL) dataset with 1° latitude/longitude horizontal grid spacing. Although cumulus parameterisation is not designed to be used at spacing smaller than about 5–10 km (Molinari and Dudek 1992), application of the modified version of the Kain and Fritsch cumulus parameterisation scheme (Kain 2004) for both domains simulates better track and intensity of tropical cyclone *Glenda*. Other physics packages include the WRF single-moment six-class microphysics scheme with graupel (WSM6; Hong et al. 2004) and the Yonsei University planetary boundary layer (YSU-PBL) scheme (Noh el al. 2003). Besides the control simulation (CTRL), two other experiments are carried out: in experiment NOTOPO the terrain elevation was set to zero everywhere, while in experiment NOLAND the earth surface was changed to water everywhere. The simulations are initiated 60 hours before the tropical cyclone reaches its maximum intensity and the duration of each of the simulations is 120 hours.

General description of the tropical cyclones

From the 2005–06 to 2009–10 seasons, six tropical cyclones made landfall in northwest Australia: *Glenda* (2006), *George* (2007), *Kara* (2007), *Nicholas* (2008), *Billy* (2009) and *Laurence* (2010). Due to the lack of radar observation for *Kara* (2007), the other five tropical cyclones are examined here (Fig. 1). Although there were some disastrous tropical cyclone landfalls in the northeastern Australian region such as tropical cyclone *Larry* (2006) and tropical cyclone *Yasi* (2011), the focus is on northwestern Australia because there are more historical landfall cases to examine such that our analysis results are more robust. Moreover, west Australia is quite a flat area with the average altitude of only about 400 m based on 1° latitude/longitude resolution topography database (indicated in Fig. 4). This represents an advantage in our analysis because our discussion can be concentrated less on the processes associated with the topography during landfall and fewer complications are induced by topographic effects. Comparatively, tropical cyclone landfalls in the northeastern Australian region are highly affected by topography at the Great Dividing Range.

These five tropical cyclones initially moved either westward or southwestward. Four of them then turned southward and made landfall in the Pilbara region of northwestern Australia. In contrast, tropical cyclone *Billy* formed near the coast of Joseph Bonaparte Gulf, moved across land over the northern Kimberley region and then back over the ocean with a northwestward track. Three of them (tropical cyclones *Glenda*, *George* and *Laurence*) made landfall almost normal to the coastline. On the other hand, tropical cyclone *Nicholas* moved to the western side of Australia, and then made landfall south of Coral Bay with a small inclination angle to the coast line.

Tropical cyclone *Glenda* formed in the Joseph Bonaparte Gulf and developed rapidly after it moved out to sea from the Kimberley coast on 27 March 2006. It moved southwestward and continued intensifying from a category 1 tropical cyclone to a category 5 tropical cyclone on 28 March 2006, and then it weakened to a category 3 tropical cyclone on 30 March 2006 as it approached the Pilbara coast. After landfall *Glenda* quickly weakened and dissipated on 31 March 2006 (Perth Tropical Cyclone Warning Center, hereafter as PTCWC 2006).

Tropical cyclone *George* also formed near the Joseph Bonaparte Gulf on 2 March 2007 as a tropical low. It moved westward across the northern Kimberley region and then offshore into the Indian Ocean on 5 March 2007. George intensified to a category 3 tropical cyclone on 7 March 2007, moved southward and attained category 5 intensity when it approached the coast on 8 March 2007. It was at its maximum intensity when it made landfall 50 km northeast of Port Hedland. Tropical cyclone *George* then continued moving inland and dissipated on 11 March. Tropical cyclone *George* was the most destructive cyclone to affect Port Hedland since tropical cyclone *Joan* in 1975 (PTCWC 2007).

Tropical cyclone *Nicholas* attained category 1 intensity on 12 February 2008. It made a loop on that day and then turned southwestward, moved almost parallel to the Pilbara coastline and intensified to a category 3 tropical cyclone. After tropical cyclone *Nicholas* moved to the north of Learmonth, it turned southward and later southeastward. It then weakened to a category 1 tropical cyclone at 0700 UTC 19 February 2008, six hours before it made landfall 60 km south of the Coral Bay and dissipated a day later (PTCWC 2008a).

Similar to tropical cyclones *Glenda* and *George*, tropical cyclone *Billy* formed in the Joseph Bonaparte Gulf on 18 December 2008. It moved across the north Kimberley region, and then further west along the coast when land effects are most prominent. Tropical cyclone *Billy* moved off shore on 23 December 2008 and its later life was entirely over the ocean.

Once the land effects decreased, its intensity increased and it became a category 4 tropical cyclone on 24 December 2008. Billy subsequently weakened to a category 2 tropical cyclone in the Indian Ocean 750 km north of Learmonth on 27 December 2008 (PTCWC 2008b).

Tropical cyclone *Laurence* developed from a tropical low within the monsoon trough in the Arafura Sea on 8 December, and reached tropical cyclone intensity on 14 December 2009. Tropical cyclone *Laurence* then moved southwestward along the Kimberley coast. Although part of the tropical cyclone was over land, *Laurence* attained category 5 intensity on 21 December 2009. It made landfall at the Pilbara coast on 21 December and eventually dissipated on 23 December (PTCWC 2009).

Asymmetries in convection and rainfall distributions

The accumulated AWAP rainfall is shown in Fig. 2, which shows the decrease of rainfall after the tropical cyclones moved inland. However, there was no gauge measurement of rainfall over the ocean and the daily data do not allow a detailed investigation on how the spatial distribution varies with time. Therefore, the IR TB from MTSAT and the rain rate estimate based on radar reflectivity are analysed. Figure 3 shows the TB at 1230 UTC 8 March 2007 and radar-estimated rain rate at 1200 UTC 8 March 2007 for tropical cyclone *George*. The TB distribution shows more deep convection northwest of the tropical cyclone centre; while radar-estimated rain rate suggests more intense rainfall southwest of the tropical cyclone centre. This difference is probably due to the downstream development of deep convection following the tropical cyclone circulation, and that IR TB measures the cirrus shield. The radar image shows the rainfall is clearly concentrated at the right side of the tropical cyclone where the flow is offshore. Similar asymmetric rain rate patterns are identified for tropical cyclones *Glenda*, *Billy* (just before it moved back to the ocean) and *Laurence* at their respective landfall times (not shown). For tropical cyclone *Nicholas*, the radar reflectivity is quite weak; however, a similar asymmetry in rainfall can still be identified.

The aforementioned asymmetries in rainfall patterns for the five tropical cyclones are clearly revealed when the accumulated rainfall patterns based on radar estimation are examined (Fig. 4). The analysis period for each tropical cyclone is determined by availability of radar observation. The radar-based accumulated rainfall over land is generally smaller than that derived from the AWAP observation. That may be due to the binned categories in radar data, but their spatial distributions are similar. An exception is tropical cyclone *Laurence* for which AWAP rainfall shows a rainfall maximum left of the track but radar estimation shows the maximum in the right side. From the radar estimation, it can be seen that for tropical cyclones *George*, *Nicholas* and *Laurence*, the maximum rainfall is concentrated to the right side of their tracks during landfall. There are two rainfall maxima for tropical cyclone *Glenda*, and at landfall time a slight asymmetry to the right of track can be identified. In contrast to the other tropical cyclones, tropical cyclone *Billy* is leaving the land when the accumulated rainfall is calculated. However, during that period, part of the tropical cyclone circulation is over land and the other over ocean, which is similar to the other landfalling tropical cyclones. Its rainfall maximum is found on the left side of the track.

To better illustrate the temporal evolution of the asymmetric structures in the five tropical cyclones, the TB and radar-estimated rain rate are displayed as a time series with respect to different azimuthal angles from the tropical cyclone centre (Figs. 5 and 6). The TB (radar) observations are first interpolated to a 20 km × 5° (2 km × 1°) polar grid centred on the tropical cyclone, and then averaged within 400 km radius. The tropical cyclone motion angle is taken as the reference azimuthal angle ('front' in Figs. 5 and 6). While there are some discontinuities in the time series due to missing satellite or radar data, the overall evolution of the convection and rainfall in the five tropical cyclones can be revealed.

As shown in Fig. 5, deep convection is more concentrated at the right (left) side of the four landfalling tropical cyclones (land-leaving tropical cyclone *Billy*). Comparison between the TB patterns in Fig. 5 and rainfall patterns in Fig. 6 indicates that the coldest TB (deepest convection) appears at azimuthal angles about 90° downstream (along the cyclonic flow) from that of maximum rainfall, which is similar to the situation in Fig. 3. To simplify the discussion, our analysis mainly focuses on the radar data. As shown in Fig. 6, most of tropical cyclone Glenda's rainfall was concentrated on its front left side initially, and then split into two areas: one stayed in the left and another shifted to the right. Although some radar data was missing (discontinuous areas in the figure), when *Glenda* was approaching land the rain intensity in the front right quadrant kept increasing. The total storm rainfall also reached its maximum during landfall. The radar data only covers tropical cyclone *George* for about ten hours when it was landfalling. The data show that tropical cyclone *George's* rainfall was concentrated in its front quadrants but with a bias to the front-right quadrant. The total storm rainfall reached its maximum just two hours before its centre moved over land. In contrast, tropical cyclone *Nicholas* had the lightest rainfall among the five tropical cyclones. When it first came into the coverage area of radars, the rainfall was mostly distributed in its front quadrants but with a slight bias to the front-left quadrant. When approaching land, its rainfall shifted to its front-right and rear-right quadrants. Tropical cyclone *Nicholas's* total storm rainfall maximum appeared about 12 hours before landfall. Tropical cyclone *Laurence* had a rather small structure: it had a gale radius of 65 km (35 nm) at 0600 UTC 21 December 2009, a storm radius of 41 km (22 nm) and a radius of maximum wind (RMW) of 33 km (18 nm). Thus, rainfall within Laurence was well covered by the radars due to its small size, and it remained in the coverage for three and half days during 18–21 December

Fig. 2. Accumulated AWAP daily rainfall (contours) and tracks during the indicated period for the five tropical cyclones, respectively.

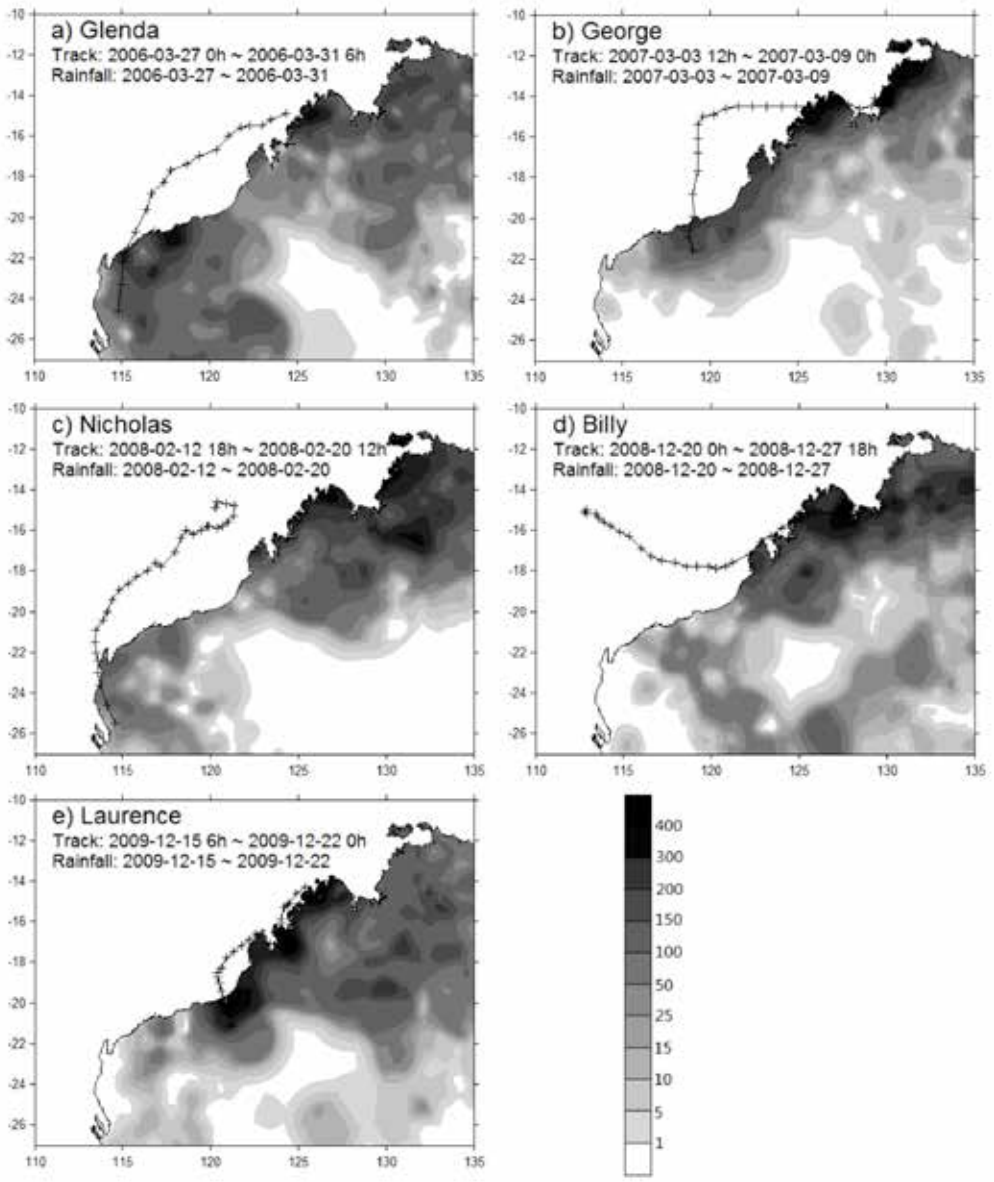

Fig. 3. (a) MTSAT IR brightness temperatures (unit: °C) at 1230 UTC 08 March 2007 for tropical cyclone *George*. The black contour indicates a temperature of –75 °C. (b) Radar-estimated rain rate (mm h^{-1}) at 1200 UTC 8 March 2007 for tropical cyclone *George* with the small box indicated in (a). Red stars indicate the locations of the radar stations.

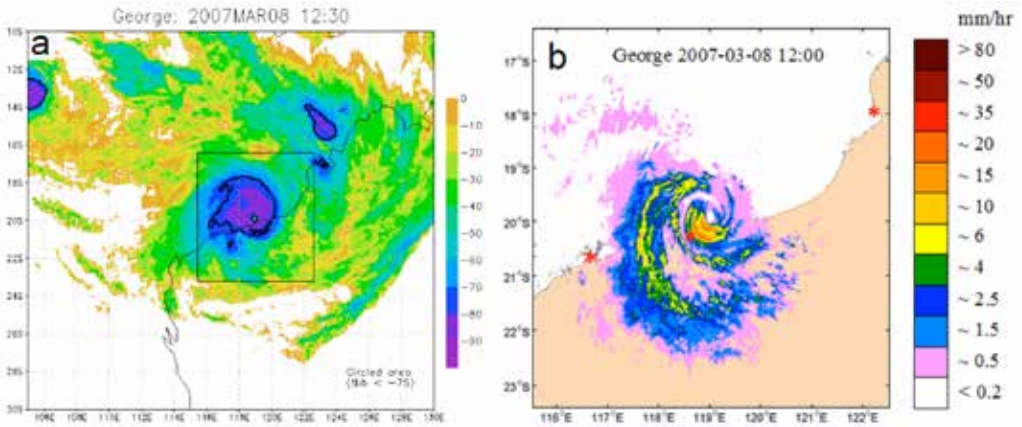

Fig. 4. Accumulated rainfall (unit: mm) based on radar estimation during landfall of the five tropical cyclones. The periods of accumulation (black portion of tracks) are approximately 40 h for tropical cyclone *Glenda*, 10 h for tropical cyclone *George*, 43 h for tropical cyclone *Nicholas*, 37 h for tropical cyclone *Billy* and 86 h for tropical cyclone *Laurence*. The contours represent topography (unit: m). Radar stations are indicated by red or white stars.

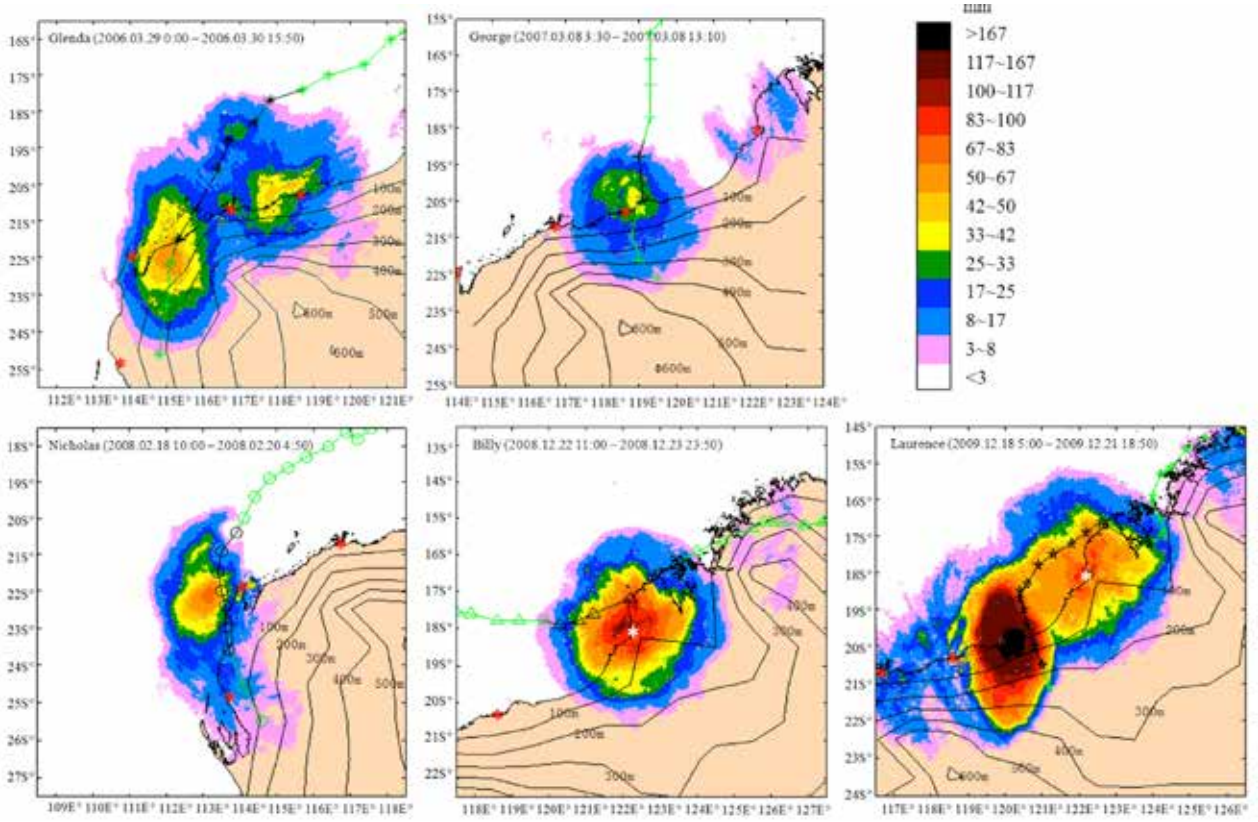

Fig. 5. Time series (abscissa) and azimuthal distribution (ordinate) of the MTSAT IR brightness temperatures (averaged up to 400 km from centre). The red line indicates the landfall time.

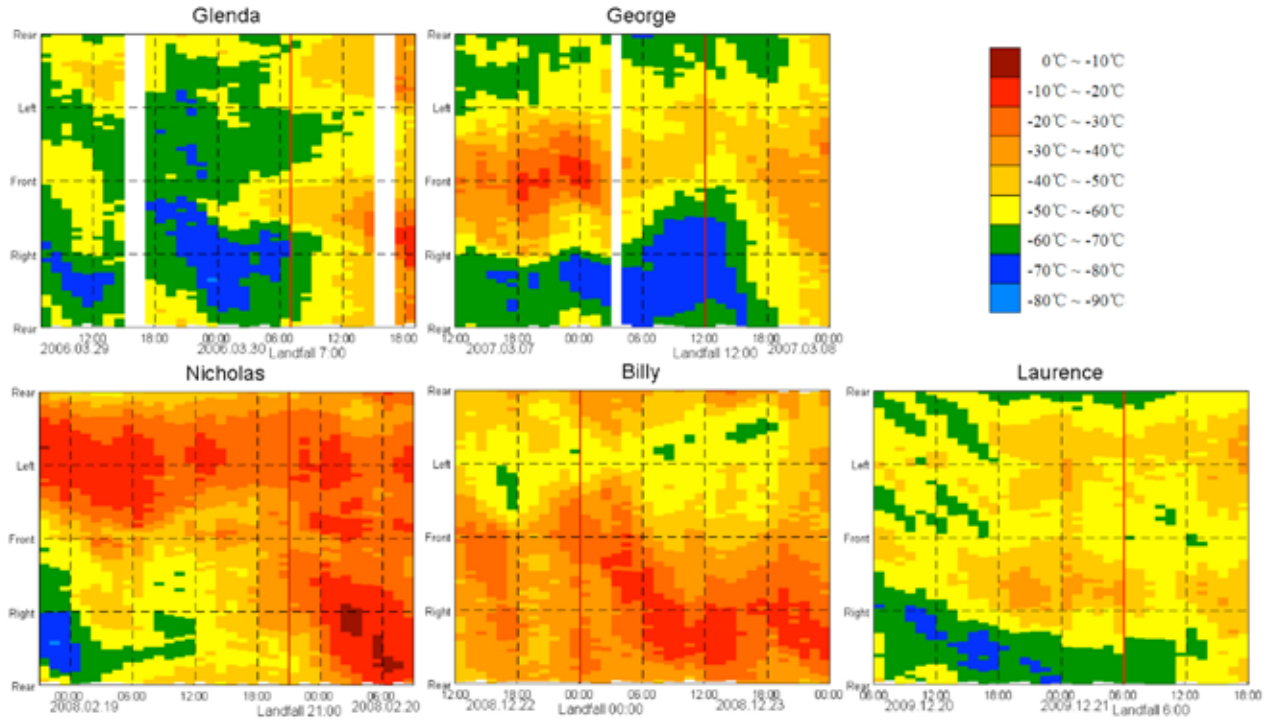

2009. Two days before landfall, tropical cyclone *Laurence's* rainfall was mainly distributed in its left quadrants. When *Laurence* was getting closer to land, its rainfall was more concentrated in the right quadrants. The storm total rainfall increased substantially a day before landfall. Tropical cyclone *Billy* is the only tropical cyclone that moved from land to the sea in our analysis. The rainfall maxima were in the front quadrants with a preference for the front-left quadrant on 22 December 2008. When *Billy* was heading to the coast from inland, the major rainfall area kept rotating from the front-left quadrant to the rear quadrants. After the tropical cyclone centre moved over sea, the rainfall areas concentrated on its left side with a preference for the rear-left quadrant. The total storm rainfall intensity increased rapidly after *Billy's* centre was over the sea surface six hours later.

In short summary, during landfall process the four tropical cyclones herein show that the major rainfall location has the tendency to occur in the left quadrants when it is over sea surface and in right quadrants when it is close to land surface. The possible physical mechanisms that lead to this asymmetry in rainfall are discussed in the following section.

Possible mechanisms responsible for the asymmetric rainfall distribution

General consideration

According to previous studies (Koteswaram and Gaspar 1956, Miller 1958), the rainfall maximum of landfalling tropical cyclones is often located in their front quadrants with a preference for the onshore side due to the effect from increased surface friction. However, at landfall the four southern hemisphere tropical cyclones analysed in this study all had their rainfall maximum located in their front-right quadrant where the cyclonic winds went offshore. For the land-leaving tropical cyclone *Billy*, the rainfall maximum was located at its left side where the winds also went offshore. The observations for these five tropical cyclones in northwestern Australia are consistent with previous studies such as Chan et al. (2004) and Liu et al. (2007). By using satellite and radar data, Chan et al. (2004) examined the landfalls of three typhoons on the south China coast, and identified enhanced convection to the western side of the tropical cyclones (i.e. side with offshore flow) starting from ~6 to 18 hours before landfall. Moreover, satellite cloud-top brightness temperature data showed enhanced convection south of the tropical cyclone centre. That is, enhanced convection occurred to the west of the tropical cyclone in the mid to lower troposphere and was then advected to the southward side by the cyclonic flow and rising motion, which is similar to the IR TB and radar-estimated rainfall pattern of each tropical cyclone showed in Figs 5 and 6. Liu et al.

Fig. 6. Time series (abscissa) and azimuthal distribution (ordinate) of the averaged (within 400 km from centre) rain rate. The red line indicates the landfall time, and the horizontal line segments represent directions of the VWS within the 6 h intervals.

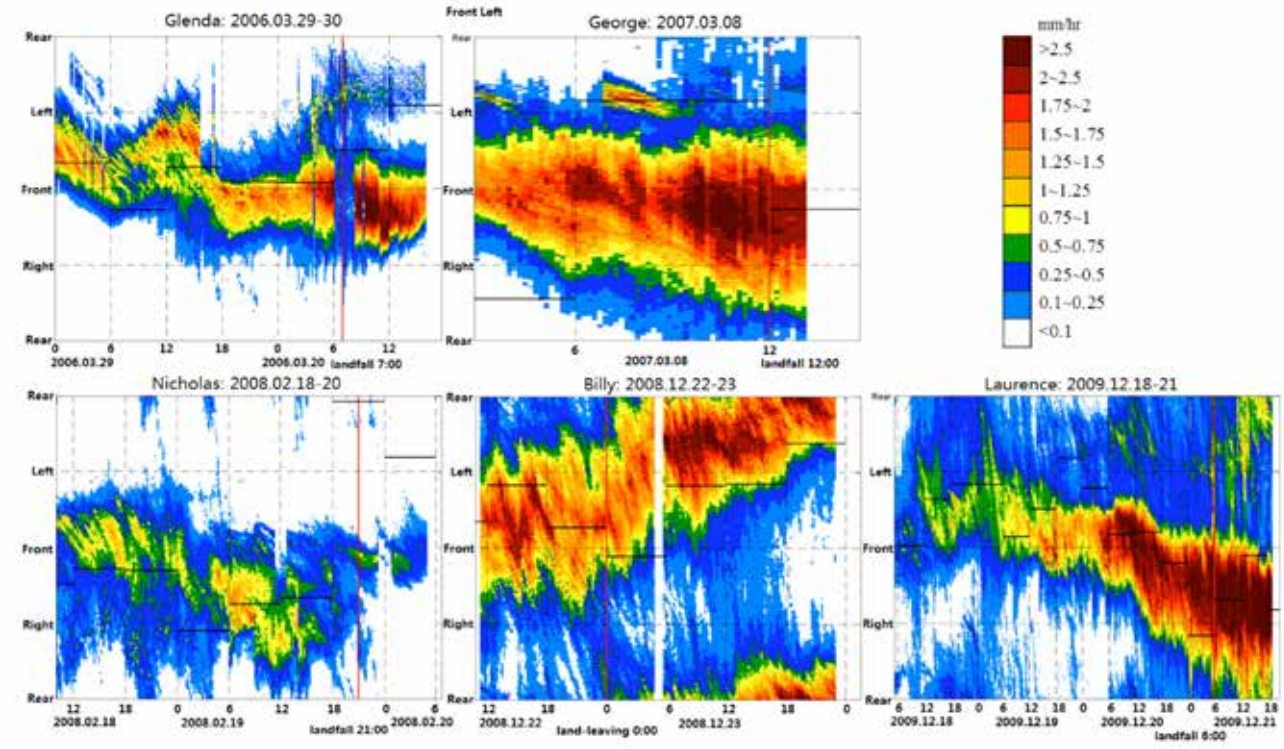

Fig. 7. Time series of the average (within 400 km from centre) 200–850 hPa VWS (unit: m s^{-1}) of the five tropical cyclones. The dashed lines indicate the times of landfall.

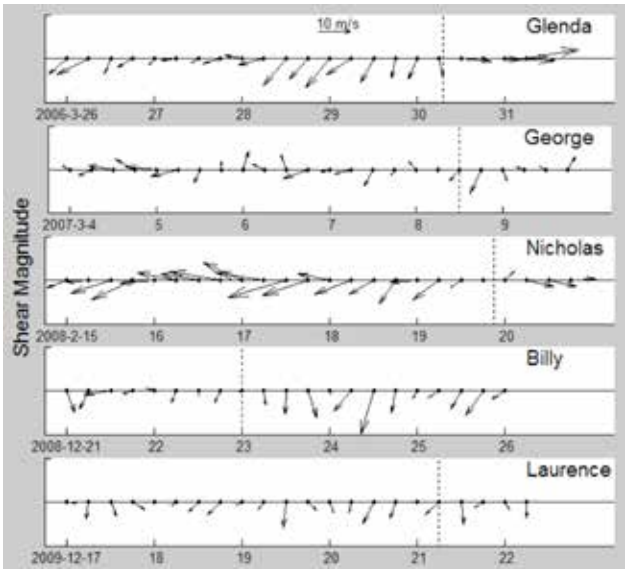

(2007) also analysed convection distribution of 18 typhoons that made landfall along the south China coast between 1995 and 2005 with satellite cloud-top brightness temperature data, and found that in ten out of the 18 typhoons convection tended to be enhanced on the western side (i.e. the offshore side) of the tropical cyclone as it made landfall, while four out of 18 on the eastern side and the four remaining cases without significant asymmetry. Powell (1982) suggested that the precipitation pattern of a tropical cyclone is not dominated by frictional convergence, but influenced by other parameters from large-scale environmental flows to local topographic effects. It is already well documented that environmental VWS tends to have a fundamental effect on the rainfall distribution (e.g. Frank and Ritchie 1999, 2001). Besides, the motion-induced and land-induced frictional asymmetry will impose rainfall asymmetry (e.g. Shapiro 1983, Kepert 2001, Kepert and Wang 2001, May et al. 2008). For some landfalling tropical cyclones, the land-sea contrast introduces rainfall asymmetry through topography effects (e.g. Ramsay 2008) and moisture supply cutoff (e.g. Chan and Liang 2003). Following this consideration, the mechanisms mentioned above are analysed in the following subsections.

Motion and VWS

Shapiro (1983) pointed out through dry numerical simulations (with a slab boundary layer model) that the motion of a tropical cyclone can induce stronger convergence in the front quadrants of the tropical cyclone, and the convergence maximum occurs in the front-right (front-left) quadrant for a northern hemisphere (southern hemisphere) tropical cyclone. The five tropical cyclones in this study had motion speeds comparable with that simulated in Shapiro (1983): tropical cyclones *Glenda*, *Nicholas* and *Laurence* were moving below 5 m s^{-1}, and tropical cyclones *George* and *Billy* had speed of 5.3 m s^{-1}. Indeed, the four landfalling tropical cyclones whose motion vectors pointed to the coast had rainfall maxima in their front quadrants. While for tropical cyclone *Billy* whose motion vector pointed to the ocean, the rainfall maximum was first in its front-left and later changed to its rear-left quadrant after the tropical cyclone centre moved over open water. The motion effect may therefore play a role in inducing asymmetries in convection in the landfall cases analysed here. However, the observed maximum rainfall is not always collocated with the motion direction of tropical cyclone *Billy* indicating the influence from other factors.

Previous observational studies such as Corbosiero and Molinari (2002) found that lightning flashes most often occurred in the front half of storms, with a preference for the right-front quadrant, while Corbosiero and Molinari (2003) also documented that for northern hemisphere tropical cyclones stronger convection prefers to occur in the downshear left region for the inner core (r < 100 km) and downshear right region for outer rainbands (r = 100–300 km). Corbosiero and Molinari (2003) pointed out the fact that motion, VWS and rainfall distribution are related with each other, and thus storm motion and VWS are themselves systematically related. However, during the time that motion and VWS had different directions, it is the VWS that tended to dominate rainfall distribution. Some other research such as the numerical study of Rogers et al. (2003) and the satellite observations of Cecil (2007) also identified stronger rainfall on the downshear-left side for northern hemisphere tropical cyclones.

However, the aforementioned studies all analysed the northern hemisphere tropical cyclones and very few studies ever examined this relationship for tropical cyclones in the southern hemisphere. The average 200–850 hPa VWS within 400 km of the tropical cyclone centre is therefore examined for the five landfall cases. Following the method used in Hanley et al. (2001), the VWS is calculated using area-weighted and azimuthally mean wind components, and thus the axisymmetric basic flow is removed. It is found from the time series of this average vertical shear that there is a prevailing northeasterly shear for all cases before landfall (Fig. 7), which is in accord with their southward or southwestward motion direction because by then the motion is left of the VWS (Corbosiero and Molinari 2003). It can be seen that for tropical cyclones *Glenda* and *Nicholas* the VWS changes to westerly after landfall, and there is a change in VWS direction as well in tropical cyclone *George* about 12 hours after landfall. Examination of the vertical variations of the wind components around landfall shows that the northeasterly shear common to all cases is mainly due to large upper-level northeasterlies, and small lower-level winds (Fig. 8). For tropical cyclones *Glenda* and *Nicholas* which went further south than the others, the increase in westerly shear and decrease in northerly shear after landfall is mainly due to enhanced low-level northeasterlies and upper-level northwesterlies.

Fig. 8. Time series of the vertical variation of wind magnitude (reference arrow of 10 m s^{-1}) and direction for tropical cyclone *Glenda*, *George*, *Nicholas*, *Billy* and *Laurence*. The solid dot indicates the landfall time.

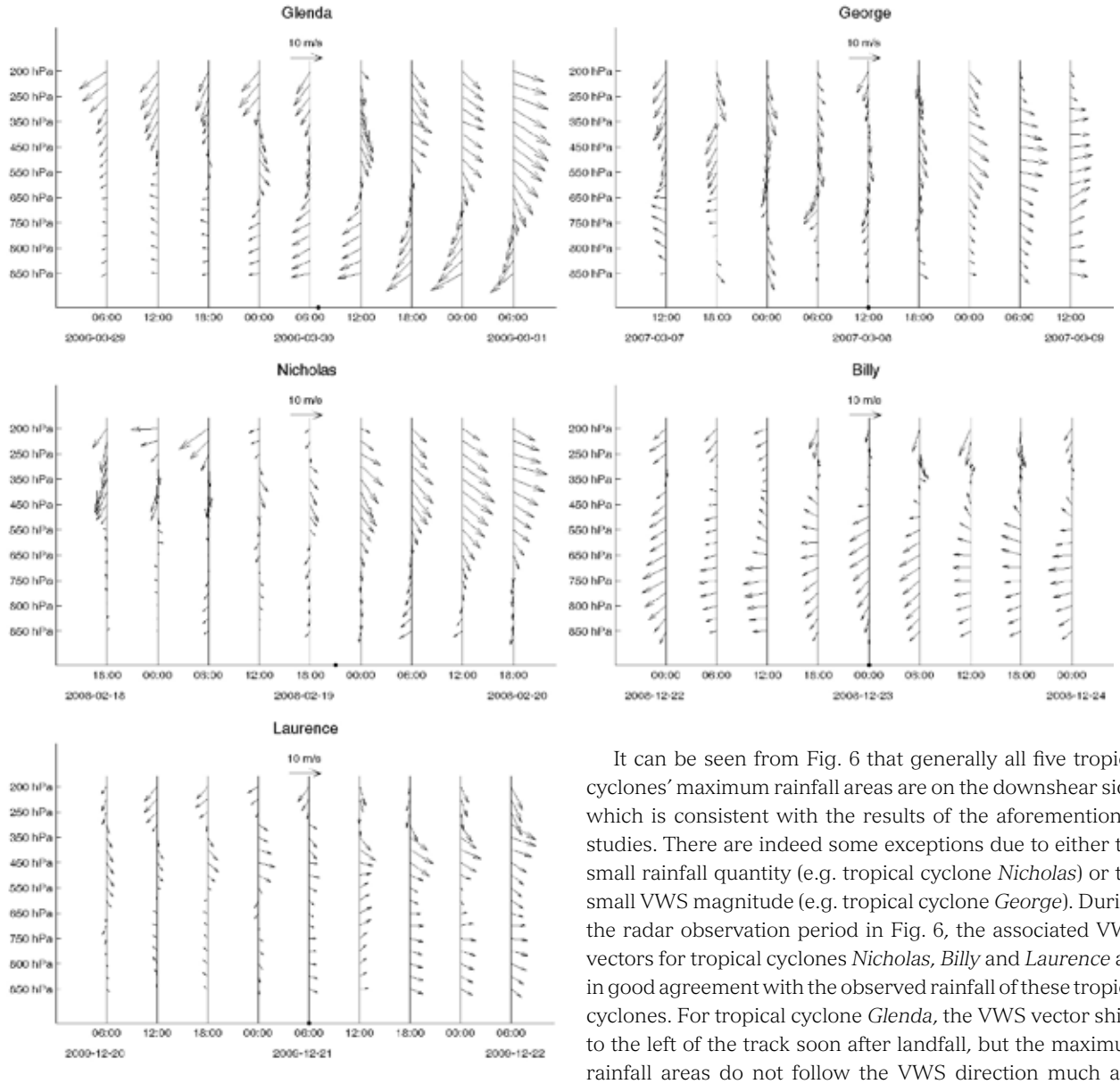

This change in VWS direction is mostly attributed to that in the environmental VWS. For example, when tropical cyclone *Glenda* travelled southwestward the prevailing 850 hPa environmental wind changed from westerly north of 15°S to easterly south of 20°S (Fig. 9). At the upper levels the 200 hPa wind changed from easterly north of 15°S to westerly south of 20°S. Thus, tropical cyclone *Glenda* experienced a change from more easterly environmental VWS before landfall to more westerly during landfall. Tropical cyclone *Nicholas* had similar change in environmental VWS except that the 850 hPa wind was not as strong as in tropical cyclone *Glenda* (not shown). These changes in the environmental wind can well explain those in the vertical wind profiles of tropical cyclones *Glenda* and *Nicholas* when they travelled about 25°S after landfall.

It can be seen from Fig. 6 that generally all five tropical cyclones' maximum rainfall areas are on the downshear side, which is consistent with the results of the aforementioned studies. There are indeed some exceptions due to either the small rainfall quantity (e.g. tropical cyclone *Nicholas*) or the small VWS magnitude (e.g. tropical cyclone *George*). During the radar observation period in Fig. 6, the associated VWS vectors for tropical cyclones *Nicholas*, *Billy* and *Laurence* are in good agreement with the observed rainfall of these tropical cyclones. For tropical cyclone *Glenda*, the VWS vector shifts to the left of the track soon after landfall, but the maximum rainfall areas do not follow the VWS direction much and remains on the right side (Fig. 6). The inconsistency here indicates that there may be other responsible mechanisms such as the frictional asymmetry due to land-sea contract.

Land-sea contrast

Chen and Yau (2003) discussed that although VWS has been known to be a dominant factor in the formation of precipitation asymmetries, the complex underlying topography and the discontinuity in the surface friction and latent heat flux also tend to generate highly asymmetric tropical cyclone structures. Through semi-idealised simulations, Chen and Yau found that the land-sea contrast provided a wavenumber–1 feature in the equivalent potential temperature field with the warm moist air to the right of the storm motion (which is almost perpendicular to land) and

Fig 9. Analysed 850 hPa and 200 hPa winds at 0000 UTC 27 March 2006 during the occurrence of tropical cyclone *Glenda*.

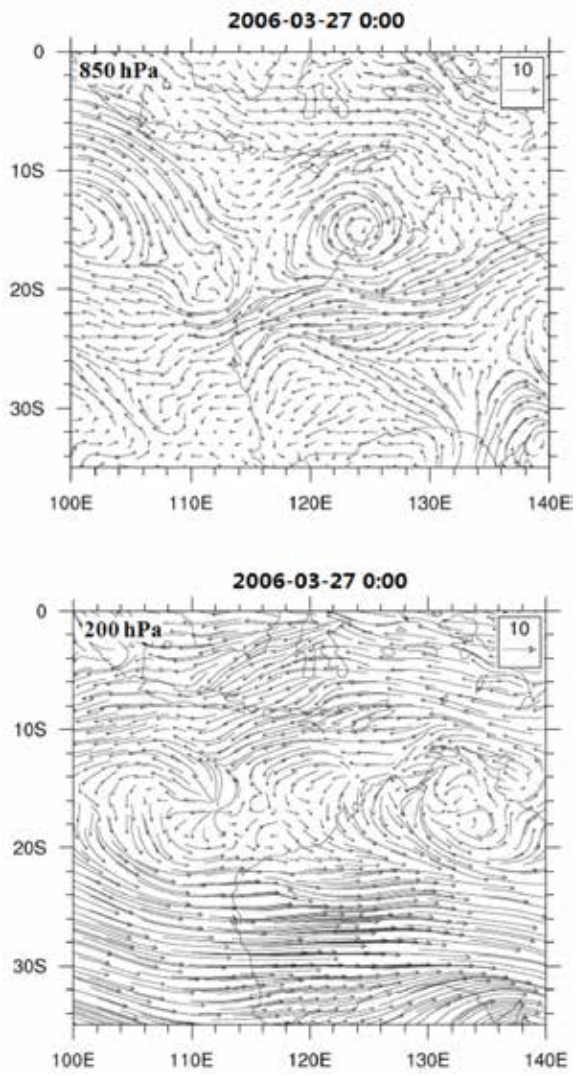

Fig. 10. Best and simulated (a) tracks and (b) surface pressure (hPa) of tropical cyclone *Glenda* for the experiments CTRL, NOTOPO and NOLAND during 1200 UTC 26 March – 1200 UTC 31 March 2006.

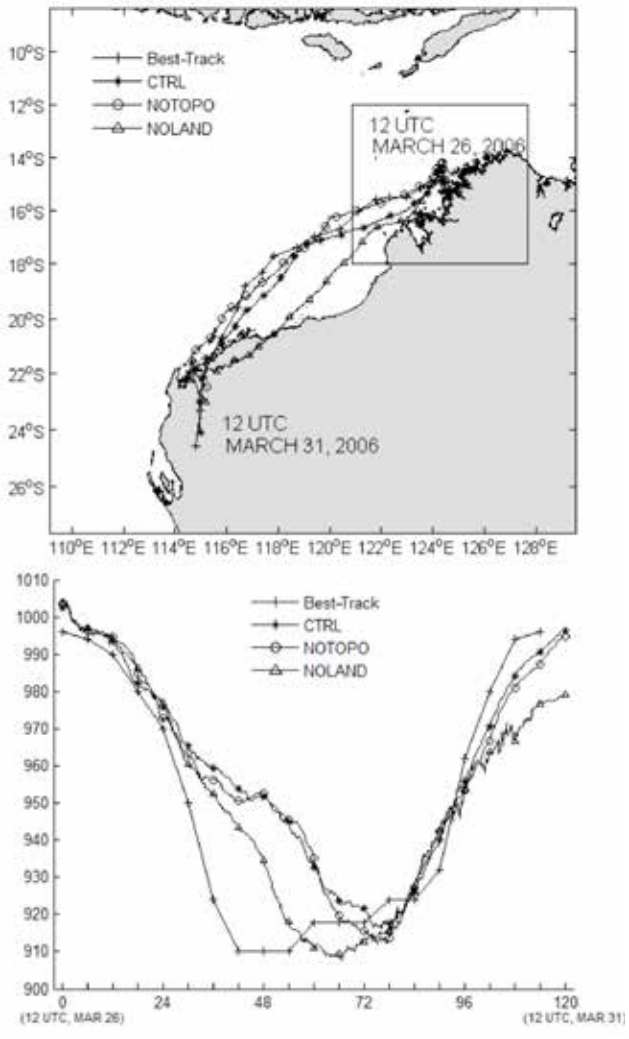

cold dry air to the left. Then low-level frontogenesis occurred and storm-scale VWS developed. The VWS vector evolved with the intensity of the storm and changed direction as the simulated tropical cyclone made landfall.

Due to the limited observations in this study, it is not feasible to determine the degree to which the rainfall asymmetry is caused by the environmental shear, and to which is caused by the land-sea surface contrast. Three numerical experiments using WRF have been carried out to further study the effects from land surface. The simulated tracks and central pressures of tropical cyclone *Glenda* from these experiments are shown in Fig. 10. In the control experiment (CTRL), the simulated tropical cyclone centre makes landfall at 103 hours (i.e. 1900 UTC 30 March 2006), while the best track shows that tropical cyclone *Glenda* makes landfall at 0700 UTC 30 March 2006. Except for this delay in landfall time, the simulated track in CTRL is in good agreement with the best track. The early stage of the simulated track in NOTOPO resembles the best track, but at later stage makes landfall more to the southwest. Without the influence from land, the simulated track in NOLAND moves southwestward from the beginning and thus deviates the most from the best track. Tropical cyclone *Glenda* experienced rapid intensification during 26 and 27 March 2006 (Fig. 10(b)). All the WRF simulations intensify the tropical cyclone to about the correct surface pressure, but fail to capture the timing of rapid intensification. Nonetheless, the weakening of the tropical cyclone during and after landfall is well simulated by both the CTRL and NOTOPO experiments. A similar rate of weakening occurs in the NOLAND experiment due to the large northwesterly VWS when the tropical cyclone travels to higher latitudes. Since there is no friction from the land surface in this experiment, the low-level environmental southeasterly is

Fig. 11. Simulated accumulated rainfall (mm) in the three WRF experiments.

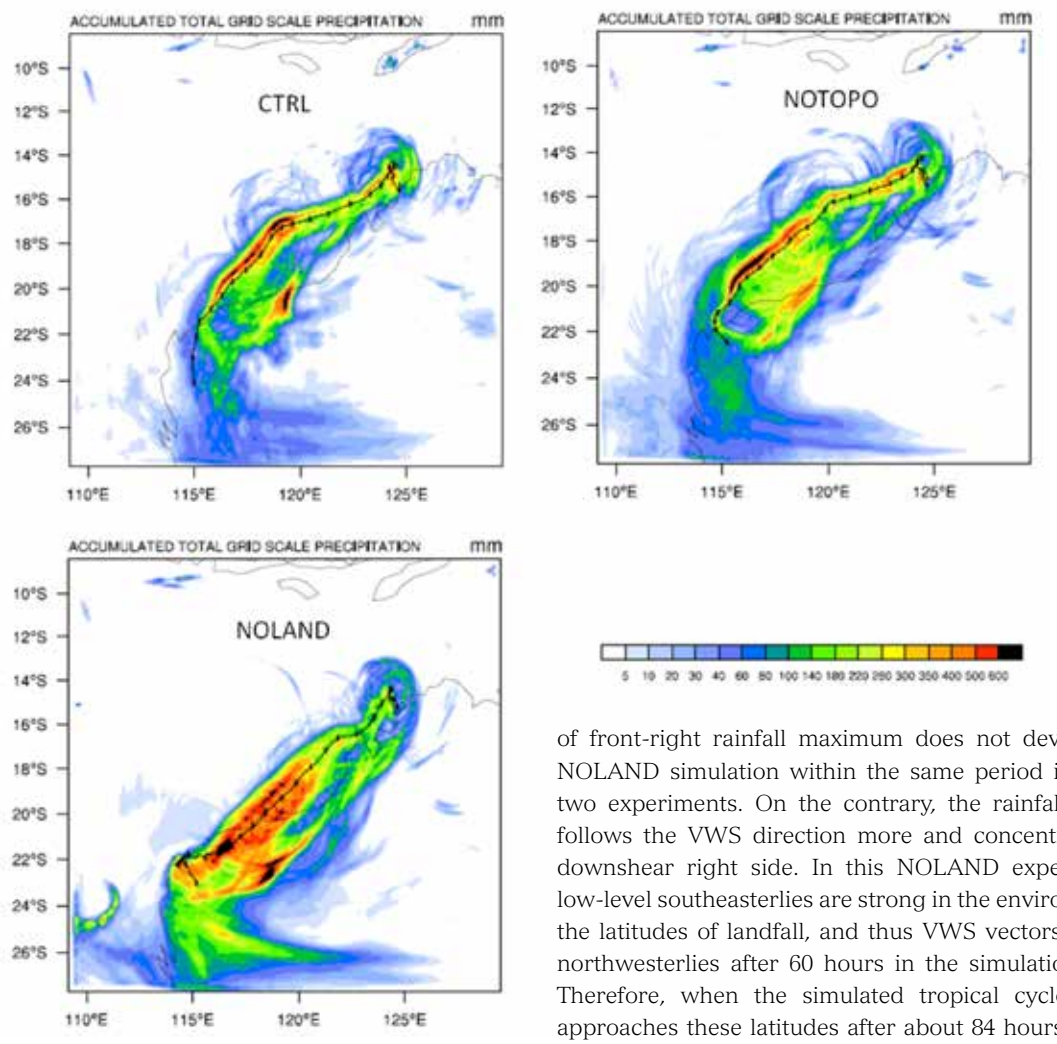

much larger than in the other two experiments (not shown).

Figure 11 shows the accumulated rainfall for the three experiments. Although the simulated accumulated rain is generally larger than that observed, it clearly indicates that in both CTRL and NOTOPO when the simulated tropical cyclone approaches land most rainfall occurs on the right side of the track, but after landfall more rainfall occurs on the left side. A large contrast is obtained in NOLAND in which the accumulated rainfall distribution is fairly symmetric with respect to the track. In other words, development of asymmetry in rainfall distribution is induced by the land-sea difference according to these simulations. To facilitate comparison with the previously discussed rainfall time series of TB and radar-estimated rain rate, similar time series of simulated rain rate are examined (Fig. 12). It can be seen that no matter whether there is a topographic effect or not (CTRL or NOTOPO), when the simulated tropical cyclone *Glenda* is about to landfall (84–96 hours), asymmetry in rainfall distribution concentrates on the right-forward side that is similar to observations. However, this asymmetry of front-right rainfall maximum does not develop in the NOLAND simulation within the same period in the other two experiments. On the contrary, the rainfall maximum follows the VWS direction more and concentrates in the downshear right side. In this NOLAND experiment, the low-level southeasterlies are strong in the environment near the latitudes of landfall, and thus VWS vectors are mostly northwesterlies after 60 hours in the simulation (Fig. 13). Therefore, when the simulated tropical cyclone *Glenda* approaches these latitudes after about 84 hours, maximum rainfall concentrates to the south of tropical cyclone centre that is right of the VWS vector.

The results from these WRF simulations imply that indeed the frictional asymmetry introduced by land surface plays its role in generating the rainfall asymmetry during tropical cyclone landfall, and it is likely that the contribution from land surface is through both storm-scale dynamics and by interaction with the environmental flow. For instance, although the simulated VWS in CTRL differs slightly from the VWS derived from CFSR data, Fig. 13 shows that the average VWS in CTRL and NOTOPO is quite different from that in NOLAND one day before landfall and afterward (actually changes from one side of the NOLAND-VWS to the other). Since it is the VWS within 400 km from centre that has been examined here, these differences in the VWS from the WRF experiments may be due to storm-scale VWS generation similar to those discussed in Chen and Yau (2003). However, with real-case simulations it is still quite difficult to isolate storm-scale processes from the synoptic-scale ones, and thus idealised simulations are more suitable to investigate these issues. As a matter of fact, some idealised

Fig. 12. As in Fig. 6 except for simulated rain rate of tropical cyclone *Glenda* in the CTRL (upper panel), NOTOPO (middle panel) and NOLAND (lower panel) experiment. The red line indicates the landfall time, and the black horizontal line segments represent directions of the VWS within the three hour intervals.

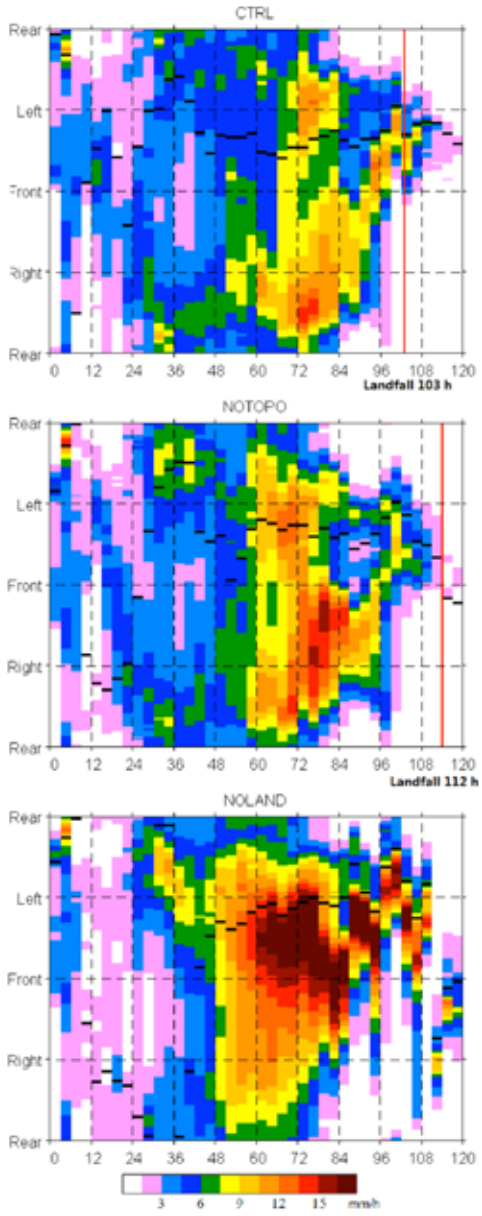

WRF simulations with quiescent environment have been performed, which show similar changes in VWS direction before and after landfall to those in Figs 7 and 8 are obtained but with smaller magnitude of changes. Whether this kind of storm-scale VWS generation is due to asymmetric convection induced by motion and boundary layer processes (Kepert 2011, Kepert and Wang 2001, May et al. 2008) and/or some other processes are under investigation. In the asymmetric convection consideration, asymmetric low-level and upper-level radial flows will be generated that result in additional VWS within the storm circulation.

Summary and concluding remarks

This study analyses five tropical cyclones that made landfall on the northwestern coast of Australia based on rain gauge data, satellite IR TB and radar-estimated rain rate. It is the first time that the spatial rainfall distribution of landfalling tropical cyclones in the southern hemisphere has been systematically investigated. The tropical cyclones are *Glenda* (2006), *George* (2007), *Nicholas* (2008), *Billy* (2009) and *Laurence* (2010). Except for tropical cyclone *Billy* that touched the coast of northwestern Australia and then moved to the South Indian Ocean, the other four tropical cyclones dissipated after landfall. Through satellite IR brightness temperatures, it is found that the distributions of deep convection are more concentrated on the right (left) side of the landfall tropical cyclones *Glenda*, *George*, *Nicholas* and *Laurence* (land-leaving tropical cyclone *Billy*). Radar-estimated rainfall more clearly reveals that at the time of landfall most of the rainfall associated with the tropical cyclones was concentrated in the front-right quadrant with respect to landfall direction. That is, instead of generating most of the rainfall on the onshore side, more rainfall was generated on the offshore-flow side of the tropical cyclones.

Potential mechanisms responsible for this observed asymmetry in rainfall distribution are discussed. Two important parameters to examine are motion and VWS, because some previous studies indicate that convective development concentrates in the front and downshear quadrants. The observed concentration of rainfall south of the tropical cyclone centres in general agrees with the motion direction. Examination of the deep-tropospheric (200–850 hPa) VWS associated with the five tropical cyclones

Fig. 13. As in Fig. 7 except for average VWS from the CFSR reanalysis data and that simulated in the three WRF experiments.

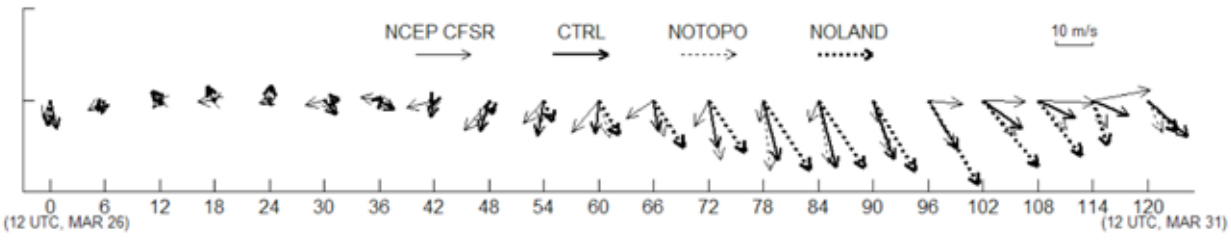

indicate that for most of the time rainfall concentrates in the downshear direction. For tropical cyclones *Glenda* and *Nicholas* that made landfall at about 25°S, the associated VWS changes from northeasterly to westerly after landfall. This change in shear is attributed to pre-landfall strong upper-level northeasterlies, and post-landfall increased low-level northeasterlies together with increased upper-level northwesterlies, which is found to be consistent with the prevailing environmental flow with strong upper-level westerly and low-level easterly south of 20°S.

However, the rainfall asymmetry of tropical cyclone *Glenda* during landfall is not totally consistent with the VWS direction. Three WRF simulations are performed that have realistic topography in CTRL, no topography in NOTOPO and an all-ocean simulation in NOLAND. While similar rainfall asymmetry with that observed is obtained in CTRL and NOTOPO, the simulated rainfall in NOLAND is mostly symmetric with respect to the tropical cyclone track. This indicates that the asymmetric friction induced by land indeed has an important role in determining the rainfall asymmetry. Because the average VWS vectors in the CTRL and NOTOPO simulations are quite different from those in NOLAND, there is the possibility of storm-scale VWS generation that has been shown in preliminary idealised simulations. Potential mechanisms behind this such as the impacts from asymmetric convection induced by motion and boundary layer processes have been discussed.

Other related processes such as changes in surface fluxes, moisture availability and instability in both boundary layer and high levels (e.g. Chan and Liang 2003) have not been examined in this study, and deserve further investigations. Several preliminary sensitivity tests with smooth land surface (roughness length changed to 10^{-4} m over land versus original value around 0.05–0.15 m) and wet land surface (moisture availability increased to 40 per cent over land versus original value around 10–15 per cent) have been performed to examine the effects induced by momentum and latent heat fluxes. It is found that the smooth land surface experiment has similar results with NOTOPO, while wet land surface experiment changes the track and rainfall distribution drastically, which indicates that moisture supply and the associated changes in vertical stability is another critical factor to consider in asymmetric convection development.

In general, the analysis results on convective asymmetries of these five landfalling tropical cyclones in the northwestern Australian region agree with previous observational and modelling studies for landfalling tropical cyclones in the northern hemisphere. As has been emphasised in the earlier discussions, the limited observations in terms of spatial and temporal resolution and available parameters do not allow us to investigate in detail the several major issues that are common to all landfalling tropical cyclones in various ocean basins. These issues include the interaction among asymmetric convection development, ambient VWS and feedbacks of tropical cyclone dynamics to the environment. Moreover, the effects of the contrast in surface fluxes between land and ocean seem to be much more complicated than previously considered (Chan 2010). While most tropical cyclones decay during landfall, some tropical cyclones can intensify when their centres moved over land. This phenomenon indicates that a land surface with increased surface friction and topography may sometimes help increase the rainfall. In particular, the sea surface temperature near coastal areas is higher than that in open ocean areas at the same latitude at summer time, which can provide more heat fluxes and enhance rainfall. A recent study by Dong et al. (2010) also found that the remnants of landfalling tropical cyclones can reinforce precipitation as they acquire energy from new sources such as baroclinic potential energy due to an intrusion of cold air or an increase of moisture transport due to monsoonal surges. To better understand these issues, idealised numerical simulations with well-controlled environments such as those in Wong and Chan (2006) will be conducted with the aim of how the aforementioned physical mechanisms work individually.

Acknowledgments

The comments and suggestions from the two anonymous reviews greatly improved the manuscript and are much appreciated. The authors would like to thank the Australian Bureau of Meteorology for providing the tropical cyclone best tracks, AWPA and radar data. The NCEP reanalysis data for this study are from the Research Data Archive, which is maintained by the Computational and Information Systems Laboratory at the National Center for Atmospheric Research (NCAR). NCAR is sponsored by the US National Science Foundation. This work utilised computational resources provided by Intersect Australia Ltd and the National Computational Infrastructure under the Merit Allocation Scheme. The first author (YL) is supported by a Macquarie University Research Excellence Scholarship (MQRES) and Higher Degree Research support fund. The second author (KKWC) acknowledges the support of the Guy Carpenter Asia-Pacific Climate Impact Centre of City University of Hong Kong where he completed a draft manuscript related to this study for his visit in February to March 2011. The work of the third author (JCLC) was supported by the General Research Fund of the HKSAR Government Grant (CityU 100210).

References

Blackwell, K.G. 2000. The evolution of Hurricane Danny (1997) at landfall: Doppler-observed eyewall replacement, vortex contraction/intensification, and low-level wind maxima. *Mon. Weather Rev., 128,* 4002–16.

Bolton, D. 1980. The computation of equivalent potential temperature. *Mon. Weather Rev., 108,* 1046–53.

Cecil, D.J. 2007. Satellite-derived rain rates in vertically sheared tropical cyclones. *Geophys. Res. Lett., 34,* L02811.

Chan, J.C.L. 2010. Changes in track and structure associated with tropical cyclone landfall. Presentation at the International Workshop on Typhoon Morakot (2009), 25–26 March, Taipei, Taiwan, Taiwan Typhoon and Flood Research Institute.

Chan, J.C.L. and Liang, X. 2003. Convective asymmetries associated with tropical cyclone landfall. Part I: f-plane simulations. *J. Atmos. Sci., 60,* 1560–76.

Chan, J.C.L., Liu, K.S., Ching, S.E. and Lai, E.S.T. 2004. Asymmetric distribution of convection associated with tropical cyclones making landfall along the South China coast. *Mon. Weather Rev., 132,* 2410–20.

Chen, Y. and Yau, M.K. 2003. Asymmetric structures in a simulated landfalling hurricane. *J. Atmos. Sci., 60,* 2294–312.

Corbosiero, K.L. and Molinari, J. 2002. The effects of vertical wind shear on the distribution of convection in tropical cyclones. *Mon. Weather Rev., 130,* 2110–23.

Corbosiero, K.L. and Molinari, J. 2003. The relationship between storm motion, vertical wind shear, and convective asymmetries in tropical cyclones. *J. Atmos. Sci., 60,* 366–76.

Dare, R.A. and Davidson, N.E. 2004. Characteristics of tropical cyclones in the Australian region. *Mon. Weather Rev., 132,* 3049–65.

Dong, M., Chen, L., Li, Y. and Lu, C. 2010. Rainfall reinforcement associated with landfalling tropical cyclones. *J. Atmos. Sci., 67,* 3541–58.

Dunn, G.E. and Miller, B.I. 1960. *Atlantic Hurricanes,* Louisiana State University Press, 377 pp.

Gao, S., Meng, Z., Zhang, F. and Bosart, L.F. 2009. Observational analysis of heavy rainfall mechanisms associated with Severe Tropical Storm Bilis (2006) after its landfall. *Mon. Weather Rev., 137,* 1881–97.

Goebbert, K.H. and Leslie, L.M. 2010. Interannual variability of northwest Australian tropical cyclones. *J. Clim., 23,* 4538–55.

Hanley, D.E., Molinari, J. and Keyser, D. 2001. A composite study of the interactions between tropical cyclones and upper tropospheric troughs. *Mon. Weather Rev., 129,* 2570–84.

Hong, S.-Y., Dudhia, J. and Chen, S.-H. 2004. A revised approach to ice microphysical processes for the parameterisation of clouds and precipitation. *Mon. Weather Rev., 132,* 103–20.

Jones, R.W. 1987. A simulation of hurricane landfall with a numerical model featuring latent heating by the resolvable scales. *Mon. Weather Rev., 115,* 2279–97.

Kain, J.S. 2004. The Kain-Fritsch convective parameterisation: An update. *J. Appl. Meteorol., 43,* 170–81.

Kepert, J.D. 2001. The dynamics of boundary layer jets within the tropical cyclone core. Part I: Linear theory. *J. Atmos. Sci., 58,* 2469–84.

Kepert, J.D. and Wang, Y. 2001. The dynamics of boundary layer jets within the tropical cyclone core. Part II: Nonlinear enhancement. *J. Atmos. Sci., 58,* 2485–501.

Koteswaram, P. and Gaspar, S. 1956. The surface structure of tropical cyclones in the Indian area. *Indian J. Meteorol. Geophys., 7,* 339–52.

Lee, C.-S., Cheung, K.K.W., Hui, J.S.N. and Elsberry, R.L. 2008. Mesoscale features associated with tropical cyclone formations in the western North Pacific. *Mon. Weather Rev., 136,* 2006–22.

Liu, K.S., Chan, J.C.L., Cheng, W.C., Tai, S.L. and Wong, P.W. 2007. Distribution of convection associated with tropical cyclones making landfall along the South China coast. *Meteorology and Atmospheric Physics, 97,* 57–68.

Lonfat, M., Rogers, R., Marchok, T. and Marks Jr., F.D. 2007. A parametric model for predicting hurricane rainfall. *Mon. Weather Rev., 135,* 3086–97.

May, P.T., Kepert, J.D. and Keenan, T.D. 2008. Polarimetric radar observations of the persistently asymmetric structure of Tropical Cyclone Ingrid. *Mon. Weather Rev., 136,* 616–30.

Miller, B. 1958. Rainfall rates in Florida hurricanes. *Mon. Weather Rev., 86,* 258–64.

Noh, Y., Cheon, W.-G., Hong, S.-Y. and Raasch, S. 2003. Improvement of the K-profile model for the planetary boundary layer based on large eddy simulation data. *Boundary Layer Meteorology, 107,* 401–27.

Parrish, J.R., Burpee, R.W., Marks Jr., F.D. and Grebe, R. 1982. Rain patterns observed by digitized radar during the landfall of Hurricane Frederic (1979). *Mon. Weather Rev., 110,* 1933–44.

Powell, M.D. 1982. The transition of the Hurricane Frederic boundary-layer wind field from the open Gulf of Mexico to landfall. *Mon. Weather Rev., 110,* 1912–32.

Powell, M.D. 1987. Changes in the low-level kinematic and thermodynamic structure of Hurricane Alicia (1983) at landfall. *Mon. Weather Rev., 115,* 75–99.

PTCWC. 2006. *Severe Tropical Cyclone Glenda,* Perth Tropical Cyclone Warning Centre, Bureau of Meteorology, 11 pp.

PTCWC. 2007. *Meteorological Aspects of Severe Tropical Cyclone George's Impact on the Pilbara,* Perth Tropical Cyclone Warning Centre, Bureau of Meteorology, 22 pp.

PTCWC. 2008. *Tropical Cyclone Nicholas,* Perth Tropical Cyclone Warning Centre, Bureau of Meteorology, 6 pp.

PTCWC. 2008. *Severe Tropical Cyclone Billy*, Perth Tropical Cyclone Warning Centre, Bureau of Meteorology, 7 pp.

PTCWC. 2009. *Severe Tropical Cyclone Laurence*, Perth Tropical Cyclone Warning Centre, Bureau of Meteorology, 13 pp.

Ramsay, H.A. and Leslie, L.M. 2008. The effects of complex terrain on severe landfalling Tropical Cyclone Larry (2006) over northeast Australia. *Mon. Weather Rev., 136,* 4334–54.

Rappaport, E.N. 2000. Loss of life in the United States associated with recent Atlantic tropical cyclones. *Bull. Am. Meteorol. Soc., 81,* 2065–73.

Rogers, R., Chen, S., Tenerelli, J. and Willoughby, H. 2003. A numerical study of the impact of vertical shear on the distribution of rainfall in Hurricane Bonnie (1998). *Mon. Weather Rev., 131,* 1577–99.

Ryan, C.J. 1993. Costs and benefits of tropical cyclones, severe thunderstorms and bushfires in Australia. *Climate Change, 25,* 353–67.

Shapiro, L.J. 1983. The asymmetric boundary layer flow under a translating hurricane. *J. Atmos. Sci., 40,* 1984–98.

Trenberth, K.E. and Guillemot, C.J. 1998. Evaluation of the atmospheric moisture and hydrological cycle in the NCEP/NCAR reanalyses. *Clim. Dyn., 14,* 213–31.

Tuleya, R.E. and Kurihara, Y. 1978. A numerical simulation of the landfall of tropical cyclones. *J. Atmos. Sci., 35,* 242–57.

Wong, M.L.M. and Chan, J.C.L. 2006. Tropical cyclone motion in response to land surface friction. *J. Atmos. Sci., 63,* 1324–37.

Yuan, J.N., Zhou, W., Huang, H.J. and Liao, F. 2009. Observational analysis of asymmetric distribution of convection associated with Tropical Cyclone Chuanchu and Prapiroon making landfall along the South China coast. *Journal of Tropical Meteorology, 25,* 101–9. (In Chinese, English abstract available).